



Contents lists available at ScienceDirect

Biochemical and Biophysical Research Communications

journal homepage: www.elsevier.com/locate/ybbrc

Dynamics of lipid droplets induced by the hepatitis C virus core protein

Rodney K. Lyn^{a,b}, David C. Kennedy^a, Albert Stolow^a, Andrew Ridsdale^a, John Paul Pezacki^{a,b,*}^a Steacie Institute for Molecular Sciences, National Research Council of Canada, Ottawa, Canada K1A 0R6^b Department of Chemistry, University of Ottawa, Ottawa, Canada

ARTICLE INFO

Article history:

Received 23 July 2010

Available online 1 August 2010

Keywords:

Hepatitis C virus
CARS microscopy
Particle tracking
Dynamics
Microtubules

ABSTRACT

The hepatitis C virus (HCV) is a global health problem, with limited treatment options and no vaccine available. HCV uses components of the host cell to proliferate, including lipid droplets (LD) onto which HCV core proteins bind and facilitate viral particle assembly. We have measured the dynamics of HCV core protein-mediated changes in LDs and rates of LD movement on microtubules using a combination of coherent anti-Stokes Raman scattering (CARS), two-photon fluorescence (TPF), and differential interference contrast (DIC) microscopies. Results show that the HCV core protein induces rapid increases in LD size. Particle tracking experiments show that HCV core protein slowly affects LD localization by controlling the directionality of LD movement on microtubules. These dynamic processes ultimately aid HCV in propagating and the molecules and interactions involved represent novel targets for potential therapeutic intervention.

Crown Copyright © 2010 Published by Elsevier Inc. All rights reserved.

1. Introduction

Hepatitis C virus (HCV) infection is a global health problem and a leading cause of liver disease [1]. HCV relies on host cell factors and molecular networks either directly by interacting with viral proteins and RNA, or indirectly by creating a favorable environment for HCV, in order to complete its' lifecycle [2,3]. HCV is a single (+)-stranded RNA virus that encodes for a single polyprotein that is cleaved into 10 proteins intrinsically divided into nonstructural (p7, NS2, NS3, NS4A-B, NS5A-B) proteins and structural proteins (core, E1, E2), each of which plays a distinct and important role in the HCV lifecycle [2]. The HCV core protein is a structural protein involved in the formation of the viral capsid and packaging of viral RNA [4]. The core protein is known to associate strongly with lipid droplets (LDs) and core is progressively loaded onto LDs overtime after HCV infection is established [4]. This association is directly correlated with the ability of HCV to produce infectious particles [5–8], making it a central player in the assembly of HCV viral particles.

The mature core protein contains two domains that control its ability to interact with LDs, stimulate fatty acid synthesis [9], induce LD biogenesis [4,10], and initiate viral particle assembly. The first domain (DI) contains highly basic amino acids that are known to interact with HCV RNA during virion morphogenesis [4,10]. The second domain (DII) is comprised of two hydrophobic

alpha helices that enable endoplasmic reticulum (ER) membrane anchoring and cytoplasmic LD association [4,10,11]. Once the mature form of core protein is released from the ER, it migrates on the surface of the phospholipid monolayer of LDs [4,10]. Pioneering work by McLauchlan and coworkers has demonstrated that HCV core protein both alters the composition of proteins bound to the LD and changes LD localization and trafficking [12]. Core also has been shown to influence host cell lipid metabolism, with HCV genotype 3a showing the most pronounced effects that have been directly implicated with inducing the biogenesis of LDs and with clinical hyperlipidemia and steatosis *in vivo* [4]. Core 3a has phenylalanine, alanine, and valine residues at positions 164, 182, and 186, respectively, and these specific amino acids have been shown to be responsible for stimulating LD biogenesis during HCV infection at the molecular level [4]. Herein, using a combination of coherent anti-Stokes Raman scattering (CARS) microscopy, differential interference contrast (DIC) microscopy, and two-photon fluorescence (TPF) microscopy combined with particle tracking techniques, we establish the dynamics of HCV core 3a protein's increase in LD biogenesis and measure directly core protein's effect on LD movement along microtubules.

2. Materials and methods

2.1. Overexpression of HCV core protein

Huh7.5 cells were seeded at 1.0×10^5 cells/well in borosilicate Lab-Tek chambers (VWR, Mississauga, ON). After 24 h, at a confluency of 60–70%, cells were transfected with core 3a plasmid

* Corresponding author at: Steacie Institute for Molecular Sciences, National Research Council of Canada, Ottawa, Canada, K1A 0R6. Fax: +1 613 941 8447.

E-mail address: john.pezacki@nrc.ca (J.P. Pezacki).

suspended in transfection media including lipofectamine 2000 (Invitrogen Canada Inc., Burlington, ON). After 4 h, DMEM in 20% FBS was added in equal volume to the chambers.

2.2. Simultaneous coherent anti-Stokes Raman scattering and two-photon fluorescence microscopies

The CARS microscopy system uses a single femtosecond Ti:sapphire oscillator as the excitation source, as previously described [13,14].

2.3. Laser scanning simultaneous two-photon excited fluorescence and differential interference contrast microscopies

An Olympus FV300 laser scanning microscopy system on an IX71 inverted microscope was used for imaging experiments. A 40× Uapo 1.15NA water immersion objective and a long working distance 0.55 NA condenser were used. The FV300 was adapted for two-photon fluorescence. Source was a Coherent Mira 900 Ti:sapphire laser producing pulses of approximately 100 fs at 800 nm wavelength with an 80 MHz repetition rate. Laser scanning microscopy can be readily adapted to DIC by taking advantage of the high inherent polarization in most laser sources. The DIC optics were adjusted as they would typically be for transmitted light use: with the prisms removed the condenser polarizer is adjusted to cross with the objective polarizer. For laser scanning, the analyzer, which is in a fluorescence cube in the IX71, is removed from the beam path. To optimally align the polarization of the laser with that of the microscope optics, a 700–1000 nm achromatic half wave plate (WPA1212 Casix) was placed in the laser path before entering the FV300 scan-box. The polarization of the laser was adjusted by rotating this wave plate to minimize the amount of light collected through the condenser polarizer. The DIC prisms are inserted and the path and the bias of the objective prism adjusted to the optimal image.

2.4. Quantitative voxel analysis

Quantitative data from the CARS images was determined using a voxel counting routine in ImageJ as previously described [15–21]. In each image, five cells were counted for a % lipid volume average.

2.5. Particle tracking of lipid droplets in Huh7.5 cells

Particle tracking of lipid droplet motion for both speed and distance was captured using spot tracker add-on with ImageJ, as previously described [22–26]. The spot tracker followed the light shaded halo contrast of lipid droplets as a result of changes in refractive index with DIC imaging.

3. Results and discussion

CARS microscopy is a convenient imaging modality for imaging changes in LD size and abundance in living cells in real time [27–33] and has previously been successfully applied to the study of HCV host-virus interactions [15–21]. Here we used CARS microscopy to measure changes in LDs induced by the expression of HCV core (genotype 3a) in Huh7.5 human hepatoma cells. We transfected a bicistronic vector expressing HCV core genotype 3a and EGFP, with separate reading frames so that EGFP marks cells that are successfully transfected and expressing HCV core protein, into Huh7.5 cells. Using simultaneous CARS and TPF microscopies, we were able to image cells overexpressing EGFP and HCV core proteins and measure changes to LD density and localization (Fig. 1, Fig. S1, supporting information) to mock transfected sam-

ples, cells that selectively express EGFP along with core protein, showed a large increase in LD size and density. The changes to LD size occurred rapidly and synchronously with the appearance of EGFP signal, typically within 8 h of transfection of the plasmid expressing the core protein.

The increase in LDs as a result of core expression was quantified by using voxel analysis [17,18], which measures the amount of lipid volume per cell, and was determined to be ~7.6% ($n = 12$), a dramatic 7-fold difference in the volume of LDs per cell. By contrast, the total lipid content in naïve cells is much lower than with core induced levels of LDs with voxel analysis yielding the lipid volume per cell to be ~1.2% ($n = 12$). Additionally, the LDs in cells lacking EGFP expression, but in cells adjacent to cells expressing EGFP and core, resemble LD size and density of mock transfected cells (Fig. 1).

After 48 h, the LDs appear to localize in the perinuclear region, where HCV replication complexes are typically found [5,34], and amass particularly close together in tight LD aggregates (Fig. 1). We observed that this change in localization occurred only after core induced the upregulation of LD biogenesis. Since the core protein is required for new viral particle assembly, eventually HCV RNA, and HCV envelope proteins must colocalize with core. Interestingly, it appears that the HCV core protein has evolved a molecular mechanism that stimulates core-associated LDs to move towards the sites of replication where new HCV RNA is produced. Here we show that this can occur very rapidly especially in the context of a real infection where viral titres can take days or weeks to reach detectable levels post-infection [7,35].

In order to perform more detailed studies of the dynamics of LD localization, we developed a new method that combines CARS, TPF and differential interference contrast (DIC) microscopies. We developed this method because we found that DIC was able to capture the movement of LDs over very long time courses (many days) without photodamaging the cells. Because LDs have a greater index of refraction than the surrounding cytosol, they can be viewed by DIC with high contrast and can be discriminated from the other organelles in the cell. We used DIC to track single LD particles and to perform kinetic measurements regarding their movement during core protein expression. To confirm that features being observed by DIC were in fact LDs, we first imaged by CARS, then superimposed those images with DIC images to identify which features in the DIC image were LDs (Fig. 2). Here we clearly observed a direct correlation between CARS signal corresponding to the C–H stretching frequency from neutral lipids contained in LDs with high contrast features captured by DIC (Fig. 2).

Next we used DIC combined with CARS and TPF microscopies to capture the movements of LDs to the perinuclear region of the cell. Following the same approach, we transfected the bicistronic vector in Huh7.5 cells. As expected, using DIC we were able to visualize an increase in number and size of LDs and also changes in localization (Fig. 3A, Movie S1, supporting information). We observed that LDs appear larger upon the appearance of EGFP fluorescence, most likely the result of core-mediated stimulation of LD biogenesis. Reorganization of LDs happens after LD enlargement reproducibly over many samples ($n = 49$). To capture LD movement we imaged many different cells with DIC right after detectable levels of EGFP expression were observed (by TPF), typically ~20 h after transfection (Fig. 1), and monitored LD redistribution with DIC for 12 h by collecting images at regular intervals. During these time course measurements, the lipid droplets appear to migrate from peripheral regions of the cell, slowly towards the perinuclear region in a period of 7 h (Fig. 3A, Movie S1, supporting information) suggest that there is a change in molecular motor driven movement of LDs that is initiated by the HCV core protein, and that this change occurs sequentially after LD biogenesis.

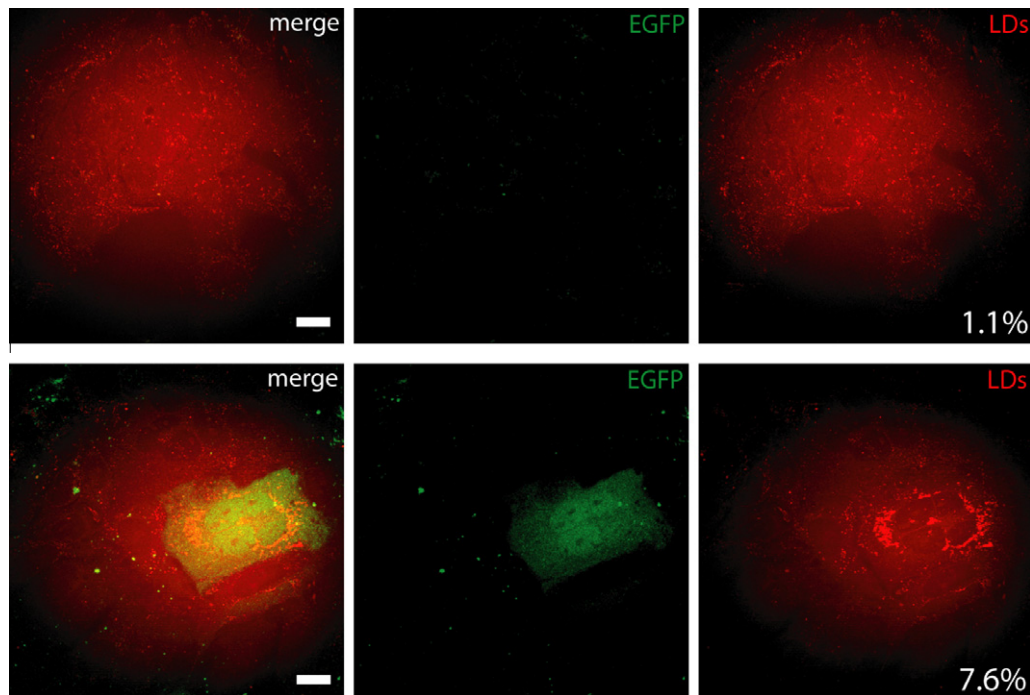


Fig. 1. Live-cell CARS microscopy imaging of lipid droplet size, density and redistribution in HCV core protein expressing Huh7.5 cells. A bicistronic plasmid encoding HCV core and EGFP was transfected into Huh7.5 cells. EGFP was used as a cellular marker for expression of core. Mock samples were incubated with lipofectamine transfection reagent without the plasmid (upper panel) and cells transfected with the bicistronic plasmid (lower panel). CAPS was used to measure LDs while TPF was used to measure EGFP. Values on the bottom of the CARS images represent voxel analysis indicating the lipid droplet volume per cell (average of 12 samples); Scale bars, 10 μ m.

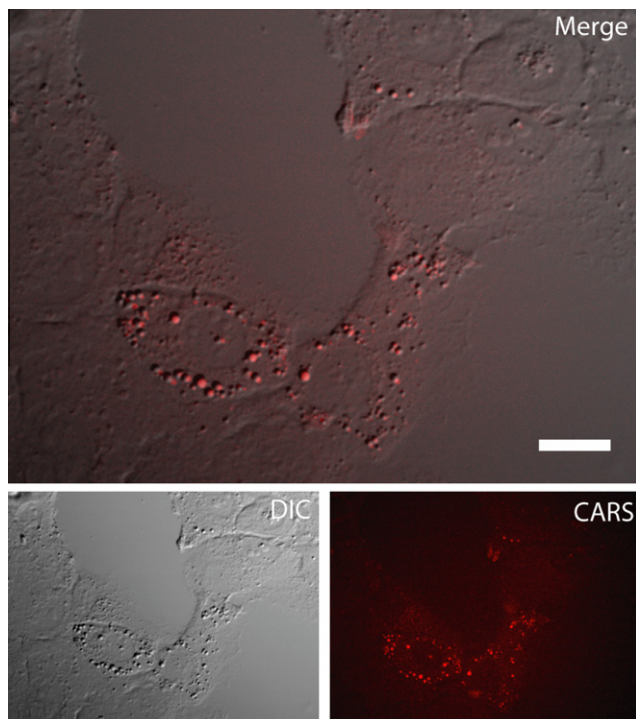


Fig. 2. Live-cell CARS and DIC microscopy imaging of HCV core protein expressing Huh7.5 cells. CARS and DIC microscopy were used to identify features that display high differential interference contrast that are rich in lipids as determined by the C–H resonance signal from CARS, shown as a merged image (upper panel). The individual CARS and DIC channels are also shown (bottom panels); Scale bars, 10 μ m.

Previous studies have shown that LDs move via a microtubule-dependant mechanism [12,36,37]. LDs also can increase in size by a

microtubule-dependent mechanism [38] or through enzymatic loading of LDs [39]. To confirm that core gives rise to changes in localization of LDs by affecting their movement along microtubules, we repeated the experiments in the presence of nocodazole, which interferes with the polymerization of microtubules [12]. First we examined LD movement of naïve Huh7.5 cells. Here, we observed that LDs move rapidly and randomly without a clear defined path. After 2 h of imaging, the same samples were treated with nocodazole. After less than 30 min after treatment, the LDs had ceased moving. These results were confirmed using CARS+TPF microscopy using a live-cell dye for labeling microtubules where continuous scanning (1.65 s intervals) demonstrated rapid movement of LDs along microtubule networks (Fig. 3B, Fig. S2 and Movie S2, supporting information). For experiments involving HCV core protein expression and nocodazole treatment we observed that the LDs increased in size due to core expression as expected but did not move to the perinuclear region as previously observed. This demonstrates that core directs the movement of randomly scattered LDs to the perinuclear region along microtubules, to where HCV replication complexes are known to reside [5,34].

It is well known that cargo movement along microtubules requires the molecular motor proteins dynein and kinesin that both anchor the cargo to microtubule tracks and move the cargo by taking step-wise movements [12,36,37,40]. LDs, like many organelles, are cargo that is transported to meet cellular demands. In order to determine the roles of the molecular motor proteins on core-mediated LD movement, we further investigated the distances traveled by LDs, under time-lapsed microscopy using DIC. Quantitative analysis was obtained via particle tracking [22–26] using pixel resolution of ~ 350 nm \times 350 nm. We tracked LD motion in naïve and HCV core protein expressing Huh7.5 cells, irrespective of directionality to assess how changes to the LD cargo may alter its motility. It is possible that movement of LD cargo along microtubules may vary according to LD size and the capacity for molecular motors to take sizeable steps before falling off the microtubule. Consistent

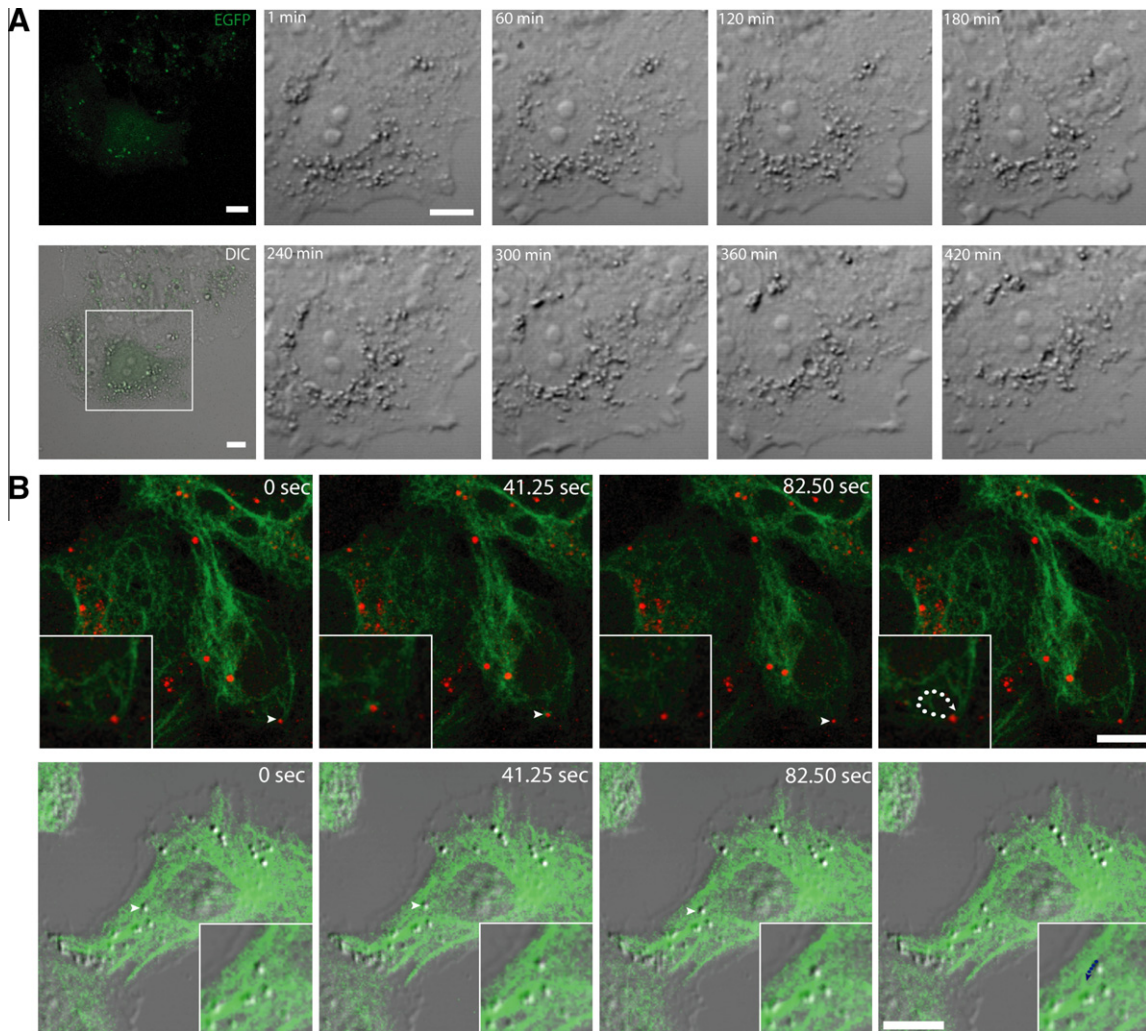


Fig. 3. Live-cell CARS, TPF and DIC microscopies were used for imaging of lipid droplet size, density and redistribution in HCV core protein expressing Huh7.5 cells. A) Migration of LDs to the perinuclear region were monitored after transfection with the bicistronic plasmid. Shown are the simultaneous TPF (upper left panel) and DIC (bottom left panel) images. The eight images are a magnified view of the white box measuring LD redistribution towards the perinuclear region within the time points indicated. Scale bars, 10 μm . B) Huh7.5 cells were stained with tubulin tracker. Simultaneous TPF and CARS (upper panel) and TPF and DIC (lower panel) microscopy were used to capture LD movement along microtubules. The white box indicates the region that is subsequently shown as a magnified view containing a region of interest with a tracked LD marked by a white arrow. The dotted line shows trajectory. Scale bars, 10 μm . (For interpretation of the references to color in this figure legend, the reader is referred to the web version of this article.)

with previous studies, we find that both the rate and average length of movement did not vary according to LD size in naïve Huh7.5 cells [12,36,37]. To assess LD motion, particle tracking was used to follow the LDs in the DIC images [22–26]. Next, changes in pixel positions in subsequent scans, 1.65 s apart, were used to project the LDs travel distance that were subsequently added together over the entire scan time (Fig. 3B). Typical experiments during live-cell imaging were conducted by monitoring the changes in displacement of a single LD throughout a 4 min continuous time course with the delay of 1.65 s per scan (Fig. 3B, Fig. S2, Movies S2 and S3, supporting information). We observed that in naïve Huh7.5 cells as well as Huh7.5 cells without the expression of HCV core (internal control) LDs move on average $17.8 \pm 0.8 \mu\text{m}$ over the time course with an average speed of $74.4 \pm 3.4 \text{ nm/s}$ ($n = 55$). By contrast, when core is expressed in these cells, the LDs move approximately half the travel distance with an average of $9.4 \pm 1.0 \mu\text{m}$ over this time period with an average speed of $39.1 \pm 4.2 \text{ nm/s}$ ($n = 51$) (Fig. 4). In comparison, LD movement in Huh7.5 cells treated with $3.3 \mu\text{M}$ nocodazole was even more hampered with the average distance traveled being only $3.7 \pm 0.1 \mu\text{m}$

with an average speed of $15.5 \pm 0.4 \text{ nm/s}$ ($n = 49$). Taken together these data indicate that core protein expression significantly affects LD motility.

When HCV core protein is translocated to LDs it forms oligomers on the LD surface and displaces LD-binding proteins such as those of the PAT family and the adipose differentiation related protein (ADRP) [4]. Movement of LD cargo on microtubules requires that molecular motor proteins dynein and kinesin bind to both the LD and the microtubule and that these molecular motor proteins are functional so that transport can take place [12,36,37]. Interactions of the core protein with the LD surface [41–43], as well as other LD-binding proteins, likely modulate the ability of dynein and kinesin to function as motor proteins. It is likely then that this change in molecular environment at the surface changes the docking environment of the LD cargo with the microtubules and gives rise to differences in speed and overall distance traveled for the LD cargo.

Previously, McLauchlan and coworkers hypothesized that correlated core-dependant LD movement may be the result of an imbalance of dynein and kinesin motors that facilitate retrograde

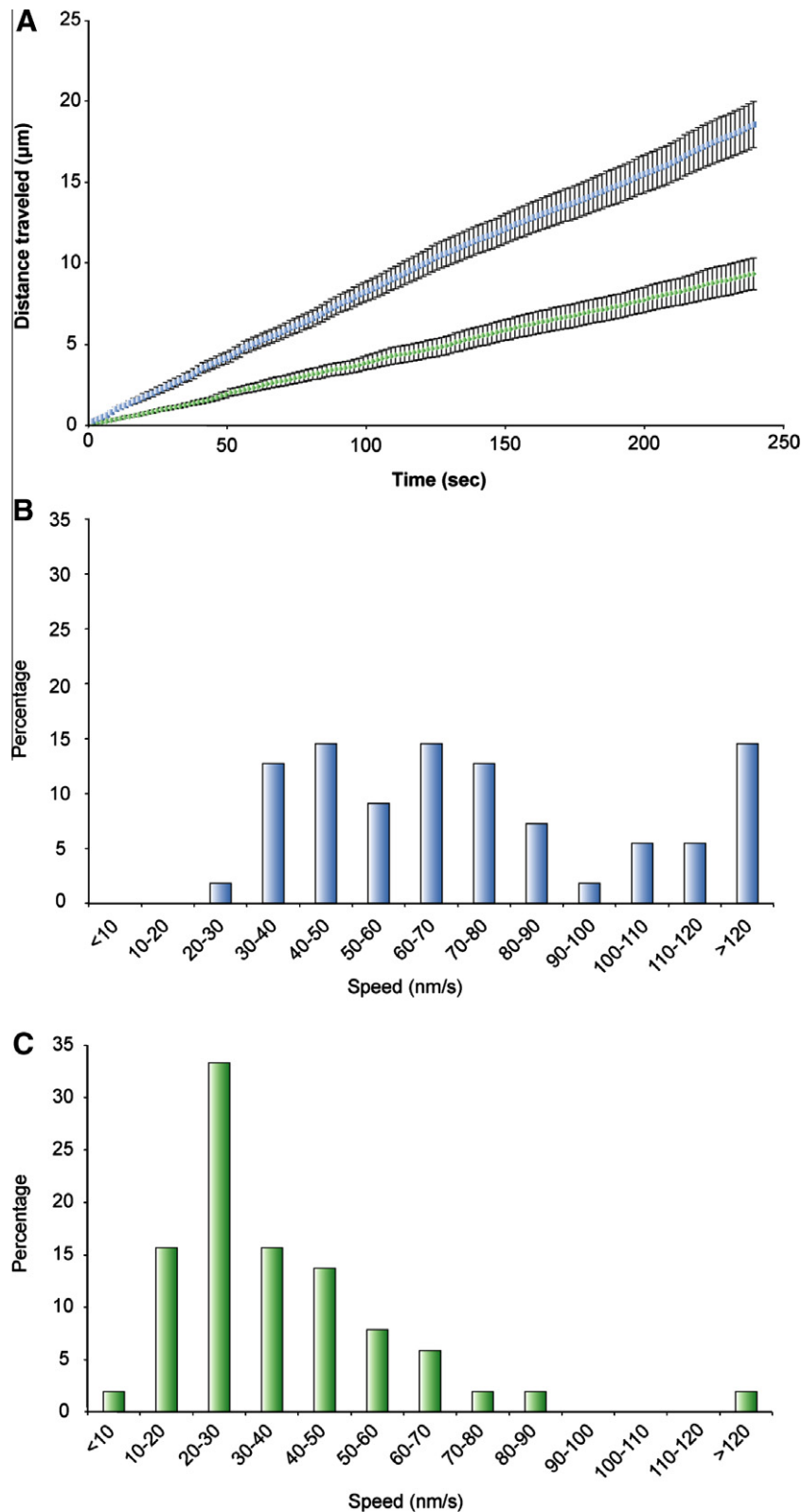


Fig. 4. Particle tracking data shows changes in speed and distance travelled by lipid droplets induced by the HCV core protein. Particle tracking of LDs was conducted using ImageJ software in Huh7.5 cells and Huh7.5 cells expressing the HCV core protein. LD movement in core expressing cells (green data points, $n=51$) and naïve Huh7.5 cells (blue data points, $n=55$) was assessed by measuring the average travel distance as a function of time (A) Particle tracking data were also plotted by using bins to represent the speed of individual LDs in naïve (B) and HCV core expressing (C) Huh7.5 cells. The binned data are for different speed increments and are expressed as a percentage relative to the sample size.

transport, possibly migrating towards the microtubule organizing center (MTOC) [4,12]. The speed measurements here show a de-

crease in molecular motor activity when the HCV core protein is expressed and binds to LDs. Since LDs are likely undergoing core-

dependent retrograde transport, preferential molecular motor activity of dynein over kinesin is likely to be taking place. There are a number of possibilities for how this could occur, however, the fact that we observe a significant decrease in the distance traveled and the speed of the LDs suggests that core is significantly reducing or eliminating the kinesin motor activity on LDs. Core may accomplish this by displacing kinesin proteins from the surface of the LDs or it may simply deactivate the kinesin through protein–protein interactions, via an allosteric mechanism. Displacing kinesin might allow for more dynein motor activity, however, our observations show that core likely eliminates half the motor protein activity, resulting in directed motion of LDs towards the perinuclear region.

4. Conclusions

In summary, we have developed a new method for particle tracking of LDs that combines DIC, TPF, and CARS microscopies. Results from imaging and particle tracking studies provide evidence that the HCV core protein controls the directionality and speed of LD movement as part of a critical step in the viral lifecycle. The substantial decrease in speed of LD movements on microtubules is likely the result of the blocking of kinesin motor protein activity. This represents a highly novel mechanism for simultaneous viral protein and host-cell organelle translocation to sites where viral particle assembly is known to take place. The core-mediated translocation of LDs also represents a novel host-HCV interaction for therapeutic intervention.

Acknowledgments

J.P.P. and A.S. thank the Canadian Institutes for Health Research (CIHR) for financial support. We thank Valerio Paziienza for HCV core expression plasmids. We thank A.F. Pegoraro, D. Moffat, and Aaron Slepokov for their assistance and useful discussions regarding CARS microscopy and particle tracking.

Appendix A. Supplementary data

Supplementary data associated with this article can be found, in the online version, at doi:10.1016/j.bbrc.2010.07.101.

References

- [1] NIH Consensus Statement on Management of Hepatitis C: 2002, NIH Consensus and state-of-the-science statements 19 (2002) 1–46.
- [2] B.D. Lindenbach, C.M. Rice, Unravelling hepatitis C virus replication from genome to function, *Nature* 436 (2005) 933–938.
- [3] J.P. Pezacki, R. Singaravelu, R.K. Lyn, Host–virus interactions during hepatitis C virus infection: a complex and dynamic molecular biosystem, *Mol. Biosyst.* 6 (2010) 1131–1142.
- [4] J. McLauchlan, Lipid droplets and hepatitis C virus infection, *Biochim. Biophys. Acta* (2009) 552–559.
- [5] D. Moradpour, F. Penin, C.M. Rice, Replication of hepatitis C virus, *Nat. Rev. Microbiol.* 5 (2007) 453–463.
- [6] S. Boulant, P. Targett-Adams, J. McLauchlan, Disrupting the association of hepatitis C virus core protein with lipid droplets correlates with a loss in production of infectious virus, *J. Gen. Virol.* 88 (2007) 2204–2213.
- [7] K. Ogawa, T. Hishiki, Y. Shimizu, K. Funami, K. Sugiyama, Y. Miyanari, K. Shimotohno, Hepatitis C virus utilizes lipid droplet for production of infectious virus, *Proc. Japan Acad. Series B-Phys. Biol. Sci.* 85 (2009) 217–228.
- [8] Y. Miyanari, K. Atsuzawa, N. Usuda, K. Watashi, T. Hishiki, M. Zayas, R. Bartenschlager, T. Wakita, M. Hijikata, K. Shimotohno, The lipid droplet is an important organelle for hepatitis C virus production, *Nat. Cell Biol.* 9 (2007) 1089–1097.
- [9] W. Yang, B.L. Hood, S.L. Chadwick, S.F. Liu, S.C. Watkins, G.X. Luo, T.P. Conrads, T.Y. Wang, Fatty acid synthase is up-regulated during hepatitis C virus infection and regulates hepatitis C virus entry and production, *Hepatology* 48 (2008) 1396–1403.
- [10] R.G. Hope, J. McLauchlan, Sequence motifs required for lipid droplet association and protein stability are unique to the hepatitis C virus core protein, *J. Gen. Virol.* 81 (2000) 1913–1925.
- [11] J. McLauchlan, M.K. Lemberg, G. Hope, B. Martoglio, Intramembrane proteolysis promotes trafficking of hepatitis C virus core protein to lipid droplets, *EMBO J.* 21 (2002) 3980–3988.
- [12] S. Boulant, M.W. Douglas, L. Moody, A. Budkowska, P. Targett-Adams, J. McLauchlan, Hepatitis C virus core protein induces lipid droplet redistribution in a microtubule- and dynein-dependent manner, *Traffic* 9 (2008) 1268–1282.
- [13] A.F. Pegoraro, A. Ridsdale, D.J. Moffatt, Y.W. Jia, J.P. Pezacki, A. Stolow, Optimally chirped multimodal CARS microscopy based on a single Ti: sapphire oscillator, *Optics Express* 17 (2009) 2984–2996.
- [14] A.F. Pegoraro, A. Ridsdale, D.J. Moffatt, J.P. Pezacki, B.K. Thomas, L.B. Fu, L. Dong, M.E. Fermann, A. Stolow, All-fiber CARS microscopy of live cells, *Optics Express* 17 (2009) 20700–20706.
- [15] X.L. Nan, A.M. Tonary, A. Stolow, X.S. Xie, J.P. Pezacki, Intracellular imaging of HCV RNA and cellular lipids by using simultaneous two-photon fluorescence and coherent anti-Stokes Raman scattering microscopies, *Chembiochem* 7 (2006) 1895–1897.
- [16] B. Rakic, S.M. Sagan, M. Noestheden, S. Belanger, X.L. Nan, C.L. Evans, X.S. Xie, J.P. Pezacki, Peroxisome proliferator-activated receptor alpha antagonism inhibits hepatitis C virus replication, *Chem. Biol.* 13 (2006) 23–30.
- [17] D.C. Kennedy, R.K. Lyn, J.P. Pezacki, Cellular lipid metabolism is influenced by the coordination environment of copper, *J. Am. Chem. Soc.* 131 (2009) 2444–2445.
- [18] R.K. Lyn, D.C. Kennedy, S.M. Sagan, D.R. Blais, Y. Rouleau, A.F. Pegoraro, X.S. Xie, A. Stolow, J.P. Pezacki, Direct imaging of the disruption of hepatitis C virus replication complexes by inhibitors of lipid metabolism, *Virology* 394 (2009) 130–142.
- [19] T. Hellerer, C. Axang, C. Brackmann, P. Hillertz, M. Pilon, A. Enejder, Monitoring of lipid storage in *Caenorhabditis elegans* using coherent anti-Stokes Raman scattering (CARS) microscopy, *Proc. Natl. Acad. Sci. USA* 104 (2007) 14658–14663.
- [20] T.T. Le, H.M. Duren, M.N. Slipchenko, C.D. Hu, J.X. Cheng, Label-free quantitative analysis of lipid metabolism in living *Caenorhabditis elegans*, *J. Lipid Res.* 51 (2010) 672–677.
- [21] I. Robinson, M.A. Ochsenkuhn, C.J. Campbell, G. Giraud, W.J. Hossack, J. Arlt, J. Crain, Intracellular imaging of host–pathogen interactions using combined CARS and two-photon fluorescence microscopies, *J. Biophotonics* 3 (2010) 138–146.
- [22] T.J. Feder, I. BrustMascher, J.P. Slattery, B. Baird, W.W. Webb, Constrained diffusion or immobile fraction on cell surfaces: a new interpretation, *Biophysical J.* 70 (1996) 2767–2773.
- [23] R.N. Ghosh, W.W. Webb, Automated detection and tracking of individual and clustered cell-surface low-density-lipoprotein receptor molecules, *Biophysical J.* 66 (1994) 1301–1318.
- [24] S.C. Kuo, J.L. McGrath, Steps and fluctuations of *Listeria monocytogenes* during actin-based motility, *Nature* 407 (2000) 1026–1029.
- [25] P.A. Sims, X.S. Xie, Probing dynein and kinesin stepping with mechanical manipulation in a living cell, *Chemphyschem* 10 (2009) 1511–1516.
- [26] R.E. Thompson, D.R. Larson, W.W. Webb, Precise nanometer localization analysis for individual fluorescent probes, *Biophysical J.* 82 (2002) 2775–2783.
- [27] C.L. Evans, X.S. Xie, Coherent anti-Stokes Raman Scattering microscopy: chemical imaging for biology and medicine, *Ann. Rev. Anal. Chem.* 1 (2008) 883–909.
- [28] J.X. Chen, A. Volkmer, L.D. Book, X.S. Xie, Multiplex coherent anti-stokes Raman scattering microspectroscopy and study of lipid vesicles, *J. Phys. Chem. B* 106 (2002) 8493–8498.
- [29] J.X. Cheng, X.S. Xie, Coherent anti-Stokes Raman scattering microscopy: instrumentation, theory, and applications, *J. Phys. Chem. B* 108 (2004) 827–840.
- [30] C.L. Evans, E.O. Potma, M. Puoris’haag, D. Cote, C.P. Lin, X.S. Xie, Chemical imaging of tissue in vivo with video-rate coherent anti-Stokes Raman scattering microscopy, *Proc. Natl. Acad. Sci. USA* 102 (2005) 16807–16812.
- [31] C.W. Freudiger, W. Min, B.G. Saar, S. Lu, G.R. Holtom, C.W. He, J.C. Tsai, J.X. Kang, X.S. Xie, Label-free biomedical imaging with high sensitivity by stimulated Raman scattering microscopy, *Science* 322 (2008) 1857–1861.
- [32] X.L. Nan, J.X. Cheng, X.S. Xie, Vibrational imaging of lipid droplets in live fibroblast cells with coherent anti-Stokes Raman scattering microscopy, *J. Lipid Res.* 44 (2003) 2202–2208.
- [33] E.O. Potma, X.S. Xie, Detection of single lipid bilayers with coherent anti-Stokes Raman scattering (CARS) microscopy, *J. Raman Spectrosc.* 34 (2003) 642–650.
- [34] B. Wolk, B. Buechele, D. Moradpour, C.M. Rice, A dynamic view of hepatitis C virus replication complexes, *J. Virol.* 82 (2008) 10519–10531.
- [35] A.I. Su, J.P. Pezacki, L. Wodicka, A.D. Brideau, L. Supkova, R. Thimme, S. Wieland, J. Bukh, R.H. Purcell, P.G. Schultz, F.V. Chisari, Genomic analysis of the host response to hepatitis C virus infection, *Proc. Natl. Acad. Sci. USA* 99 (2002) 15669–15674.
- [36] S.P. Gross, M.A. Welte, S.M. Block, E.F. Wieschaus, Dynein-mediated cargo transport in vivo: a switch controls travel distance, *J. Cell Biol.* 148 (2000) 945–955.
- [37] G.T. Shubeita, S.L. Tran, J. Xu, M. Vershinin, S. Cermelli, S.L. Cotton, M.A. Welte, S.P. Gross, Consequences of motor copy number on the intracellular transport of kinesin-1-driven lipid droplets, *Cell* 135 (2008) 1098–1107.
- [38] P. Bostrom, M. Rutberg, J. Ericsson, P. Holmdahl, L. Andersson, M.A. Frohman, J. Boren, S.O. Olofsson, Cytosolic lipid droplets increase in size by microtubule-dependent complex formation, *Arterioscler. Thromb. Vasc. Biol.* 25 (2005) 1945–1951.

- [39] D.R. Blais, R.K. Lyn, M. Joyce, Y. Rouleau, R. Steenbergen, N. Barsby, I.F. Zhu, A.F. Pegoraro, A. Stolow, D.L. Tyrrell, J.P. Pezacki, Activity-based protein profiling identifies a host enzyme, carboxylesterase 1, which is differentially active during hepatitis C virus replication, *J. Biol. Chem.* 285 (2010) 25602–25612.
- [40] N. Hirokawa, Kinesin and dynein superfamily proteins and the mechanism of organelle transport, *Science* 279 (1998) 519–526.
- [41] C. Hourieux, M. Ait-Goughoulte, R. Patient, D. Fouquenot, F. Arcanger-Doudet, D. Brand, A. Martin, P. Roingeard, Core protein domains involved in hepatitis C virus-like particle assembly and budding at the endoplasmic reticulum membrane, *Cell. Microbiol.* 9 (2007) 1014–1027.
- [42] P. Roingeard, C. Hourieux, Hepatitis C virus core protein, lipid droplets and steatosis, *J. Viral Hepat.* 15 (2008) 157–164.
- [43] Y. Rouille, F. Helle, D. Delgrange, P. Roingeard, U. Voisset, E. Blanchard, S. Belouzard, J. McKeating, A.H. Patel, G. Maertens, T. Wakita, C. Wychowski, J. Dubuisson, Subcellular localization of hepatitis C virus structural proteins in a cell culture system that efficiently replicates the virus, *J. Virol.* 80 (2006) 2832–2841.